Reports on Progress in Physics

PAPER

RECEIVED
27 January 2026

REVISED
2 April 2026

ACCEPTED FOR PUBLICATION
27 May 2026

PUBLISHED
23 June 2026

Vortex solitons in disclination quasicrystals

Hua Zhong[1], **Yaroslav V Kartashov**[2], **Yongdong Li**[1], **Fangwei Ye**[3,4,*] **and Yiqi Zhang**[1,5,*]

[1] Key Laboratory for Physical Electronics and Devices, Ministry of Education, School of Electronic Science and Engineering, Xi'an Jiaotong University, Xi'an 710049, People's Republic of China
[2] Institute of Spectroscopy, Russian Academy of Sciences, Troitsk, Moscow 108840, Russia
[3] School of Physics, Chengdu University of Technology, Chengdu 610059, People's Republic of China
[4] School of Physics and Astronomy, Shanghai Jiao Tong University, Shanghai 200240, People's Republic of China
[5] State Key Laboratory of Human-Machine Hybrid Augmented Intelligence, Institute of Artificial Intelligence and Robotics, Xi'an Jiaotong University, Xi'an 710049, People's Republic of China
[*] Authors to whom any correspondence should be addressed.

E-mail: fangweiye@sjtu.edu.cn and zhangyiqi@xjtu.edu.cn

Keywords: quasicrystals, disclination, vortex solitons

Supplementary material for this article is available online

Corresponding editor: Dr Paul Mabey

Abstract

Quasicrystals are ubiquitous in nature. They represent unique aperiodic materials featuring long-range order that occupy an intermediate niche between exactly periodic and disordered materials. These properties are reflected in the unusual evolutionary dynamics of excitations and unique localization properties of linear eigenmodes supported by quasicrystals. In particular, being the structures characterized by discrete rotational symmetry $\mathcal{C}_\nu$ of order ν, photonic quasicrystals can support the stable propagation of linear vortex-carrying light beams and vortex solitons. However, the impact of discrete rotational symmetry ν of quasicrystals on the properties of vortex light states has not been investigated so far, as only the systems constructed using the simplest Penrose tiling or corresponding optically induced Penrose lattices are considered in this context. Here, we propose a broad class of quasicrystals with global topological defects—disclinations—introduced into their structure that allows to produce novel quasicrystalline structures with any desired order of discrete rotational symmetry from the basic Penrose structure. Such global topological deformation substantially enriches the linear spectrum of quasicrystals, allowing them to support new types of linear vortex states and bifurcating from them families of stable thresholdless vortex solitons with unusual intensity and phase distributions. We find two different classes of stable vortex solitons comprising in-phase or out-of-phase pairs of closely located bright spots, with total intensity distribution reflecting a particular discrete rotational symmetry of the quasicrystal with disclination. Remarkably, even low-charge vortex solitons can be stable in quasicrystals with disclinations, whereas stability intervals for them broaden with the decrease of the discrete rotational symmetry $\mathcal{C}_\nu$ of quasicrystals. Our results extend the theory of localization in quasicrystals to structures with global topological deformation, highlighting emerging prospects for the robust transmission of power or information arising in these systems.

1. Introduction

Quasicrystals, as aperiodic structures featuring long-range order, occupy a special and crucial niche among inhomogeneous materials due to their unique internal structure and symmetry, which are directly manifested in the localization and transport properties of excitations. These characteristics, markedly different for quasicrystals, periodic (crystalline), or disordered inhomogeneous media, stem from qualitatively different localization properties and the structure of the spectrum of linear eigenstates of these media that are manifested in different physical phenomena. Among the models of quasicrystals is a celebrated aperiodic tiling suggested by Penrose [1] that played a central role in the interpretation

of scattering experiments in quasicrystalline materials [2]. Despite the absence of translational symmetry, quasicrystals, nevertheless, are characterized by a certain discrete rotational symmetry $\mathcal{C}_\nu$, which may substantially affect various physical phenomena encountered in such systems [3–5].

As versatile functional materials, quasicrystals have been explored in diverse areas of physics, ranging from condensed matter physics [6–8], physics of matter waves [9], optics [10–18], and acoustics [19, 20], to name just a few. Aperiodic moiré lattices obtained by the superposition of two mutually twisted identical sublattices that have attracted considerable attention [21–24] can also be transformed into quasicrystals, but only for specific twist angles. However, compared to moiré lattices that inherit discrete rotational symmetry from their sublattices, quasicrystals (in particular, optically induced ones) may feature any discrete rotational symmetry $\mathcal{C}_\nu$. The remarkable property of both aperiodic moiré lattices [21] and quasicrystals [15] is the delocalization-localization transition for the eigenmodes occurring in them upon the variation of the properties of the underlying aperiodic potential (in the 1D case, this effect has been demonstrated in quasiperiodic lattices [25]).

Particularly intriguing in this respect is the propagation of vortex-carrying excitations with nonzero orbital angular momentum in aperiodic quasicrystals [26, 27]. Their evolution dynamics is expected to change qualitatively when the quasicrystal is above or below the delocalization-localization transition threshold, whereas discrete rotational symmetry should impose restrictions on the maximal topological charge of excitations that can be transmitted in a stationary manner in $\mathcal{C}_\nu$-symmetric materials, leading to the dynamical splitting of phase singularities in states that do not satisfy these restrictions [28–30]. The advantage of optical materials is that their response in addition can be strongly nonlinear, allowing us to consider the rich interplay between light refraction in inhomogeneous optical potentials and nonlinear self-action. For example, in periodic nonlinear lattices, such an interplay leads to the formation of stable vortex lattice solitons [31–35], which, however, exist only above a considerable power threshold (see also reviews [36–42]). The formation of vortex solitons in aperiodic lattices is considerably less studied and requires detailed investigation, as it may create potential approaches for controlling the propagation dynamics and internal structure of light beams with nontrivial phase structure.

Although beam localization in nonlinear photonic quasicrystals and the development of vortex solitons have been considered in Penrose structures with a specific fixed discrete rotational symmetry $\mathcal{C}_\nu$ [43–49], there is still no conclusion whether the aperiodicity of the material can make such solitons thresholdless and how the discrete rotational symmetry of the quasicrystal affects the properties and stability of the nonlinear vortex-carrying excitations. In particular, all vortex solitons reported so far in Penrose quasicrystals were found to exist only above considerable power thresholds.

To answer the fundamental open question about the types of vortex solitons that can exist in a stable form in quasicrystals with variable discrete rotational symmetry, in this work we have designed a class of quasicrystals with controllable global topological deformation that can be introduced into such structures to continuously alter their discrete rotation symmetry $\mathcal{C}_\nu$. To achieve this, we use the approach that creates topological disclination [50–53] and is frequently employed in the design of higher-order topological insulators from periodic lattices [54–56], but apply it here to aperiodic Penrose quasicrystals. In the frames of this approach, the removal or insertion of μ (here $\mu \leqslant \nu - 3$) angular sectors with a Frank angle $\theta = 2\pi/\nu$ from original $\mathcal{C}_\nu$ quasicrystal lattice and their subsequent filling with waveguides allows to create disclination quasicrystals with novel discrete rotational symmetries of the order $\mathcal{C}_{\nu+\mu}$ or $\mathcal{C}_{\nu-\mu}$, overcoming limitations on the position of waveguides imposed by Penrose tiling. Notice that while formally for $\mu = 3$ one can even construct a $\mathcal{C}_2$ quasicrystal from $\mathcal{C}_5$ one, the former appears too sparse (due to the large spacing between waveguides) and does not support vortex states. The resulting quasicrystals with global topological deformation can support new types of linear vortex states and vortex solitons with symmetries not accessible neither in periodic media nor in usual quasicrystals. We encounter two different classes of vortex solitons consisting of in-phase and out-of-phase pairs of closely located bright spots, with intensity distributions featuring the same discrete rotational symmetry as the underlying quasicrystal. Corresponding *in-phase* and *out-of-phase* vortex solitons bifurcate from proper combinations of linear modes of disclination quasicrystals that are well-localized spatially for sufficiently deep optical potentials (above the delocalization-localization transition). Since such solitons bifurcate from localized linear eigenstates, they are thresholdless and feature enhanced stability. We demonstrate that stability regions are wider in quasicrystals with $\mathcal{C}_{4,5}$ discrete rotational symmetries compared to $\mathcal{C}_{6,7}$ quasicrystals. Thus, the introduction of topological disclinations allows to generate various stable vortex solitons with tailored profiles in aperiodic optical systems.

Our findings are conceptually different from the quasicrystalline linear vortex lattices that can be generated by optical induction in free space [57–59] since we consider the evolution of localized vortex inputs in a prefabricated quasicrystalline optical potential in a nonlinear medium.

2. Results

2.1. Quasicrystals with disclinations

The propagation dynamics of a light beam along the z axis in the material with focusing nonlinearity and an imprinted quasicrystal refractive index landscape are described by the dimensionless nonlinear Schrödinger equation for the amplitude of the light field ψ:

$$\mathrm{i}\frac{\partial\psi}{\partial z} = -\frac{1}{2}\nabla^2\psi - \mathcal{R}(x,y)\,\psi - |\psi|^2\psi, \tag{1}$$

where $\nabla^2 = \partial_x^2 + \partial_y^2$ is the transverse Laplacian, x and y denote the normalized transverse coordinates, and the function $\mathcal{R}(x,y)$ describes an optical potential defining quasicrystal that can be constructed from super-Gaussian functions:

$$\mathcal{R}(x,y) = p\sum_{m,n} \mathrm{e}^{-\left[(x-x_{m,n})^2+(y-y_{m,n})^2\right]^2/d^4} \tag{2}$$

with $(x_{m,n}, y_{m,n})$ denoting the coordinates of the quasicrystal sites, $p = 12$ representing the depth of the optical potential, and $d = 0.5$ being the waveguide width. Equation (1) is mathematically analogous to the canonical Schrödinger equation in quantum mechanics, with the propagation distance z playing the role of the evolution time and the field amplitude ψ being analogous to the quantum-mechanical wavefunction. Remarkably, the use of the continuous model (1) allows us to account for *all* possible types of couplings in quasicrystals, which is especially important from the point of view of accurate characterization of the structure of the linear spectrum of the system.

We start by constructing a quasicrystal using the famous Penrose tiling of the plane. The sites of such quasicrystal correspond to vertices of tiles of two types, 'thin' and 'thick' rhombuses, which are shown to have pink and green colors in schematics, respectively, in figure 1. Throughout this work, we set the edge lengths of rhombuses to $a = 2.5$. The resulting aperiodic quasicrystal is characterized by a long-range order, with similar elements appearing after nonequal distances and with $\mathcal{C}_5$ discrete rotational symmetry. Although we use the scale $a = 2.5$ to present this work's results, they remain qualitatively similar for other values of parameter a (to avoid overlap of the waveguides, a should exceed approximately 1.5, as it is required, for example, in fs-laser writing technology). The decrease of this parameter is accompanied by an increase of the coupling strength between waveguides and an overall broadening of the linear spectrum (figure 2). Thus, the eigenvalues of the modes giving rise to vortices shift upon the variation of a, but they remain in the same parts of the spectrum, that is, their structure does not change qualitatively.

To go beyond the $\mathcal{C}_5$ symmetry inherent to the Penrose tiling, we introduce disclination defects by removing or adding into the above structure μ sectors with Frank angle $\theta = 2\pi/5$ (denoted with yellow region in figure 1) and adjust the position of all remaining sites by uniformly stretching or compressing the structure to fill the removed sector or to accommodate the added one. This yields representative quasicrystals with global topological defects having, for example, $\mathcal{C}_4$ or $\mathcal{C}_6$, $\mathcal{C}_7$ discrete rotational symmetry (see the bottom row of figure 1) and different central (core) regions. Using this method, one can in principle produce an entire class of disclination quasicrystals with symmetry ranging from $\mathcal{C}_3$ to $\mathcal{C}_\infty$. Furthermore, we concentrate on light propagation in quasicrystals with discrete rotational symmetry from $\mathcal{C}_4$ to $\mathcal{C}_7$. Corresponding refractive index distributions $\mathcal{R}(x,y)$ in these structures are shown in figures 2(a)–(d). To limit the number of modes under consideration, we further assume that these structures are sufficiently large, but finite (i.e., sixth-order Penrose tiling was used as a 'parent' structure in all cases). In the supplemental material, we display other degenerate states that can form vortex states with higher topological charges.

Such structures can be created by using the method of fs-laser writing of waveguides in transparent dielectrics [60–68], optical induction technique with sets of interfering plane waves in photorefractive crystals [11, 13, 21, 69–72] and atomic vapors [73, 74], and various other techniques [10, 75]. For details of the normalizations employed in equation (1), see [17, 66].

2.2. Linear spectra and modes of quasicrystals

To understand how the introduction of topological disclination changes the spectrum of quasicrystals, it is instructive to consider the linear spectra of eigenmodes of the corresponding structures. Such eigenmodes are found from equation (1) in the form $\psi(x,y,z) = u(x,y)\mathrm{e}^{\mathrm{i}bz}$, where b denotes the propagation constant (eigenvalue) and $u(x,y)$ is the real function describing the mode profile. Such profiles satisfy

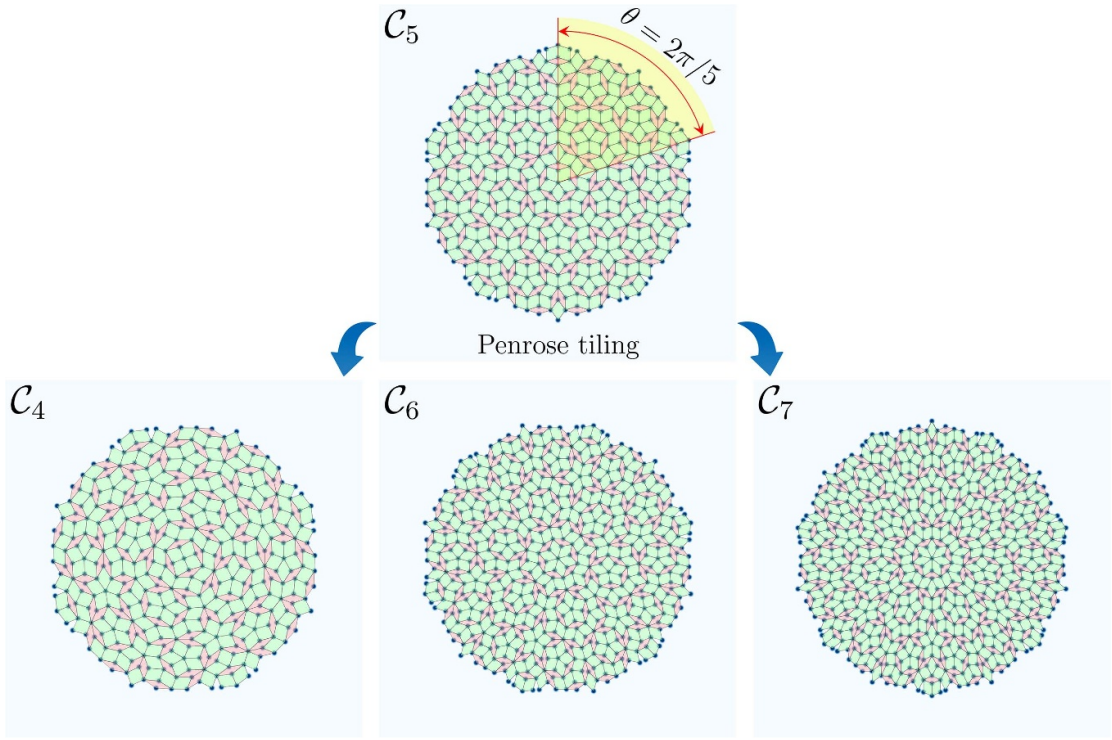

Figure 1. Quasicrystals obtained using Penrose tiling (top) and its disclination counterparts (bottom) with different discrete rotational symmetries $\mathcal{C}_\nu$. The yellow sector with the Frank angle of $\theta = 2\pi/5$ can be removed or added into the structure to introduce disclination defect.

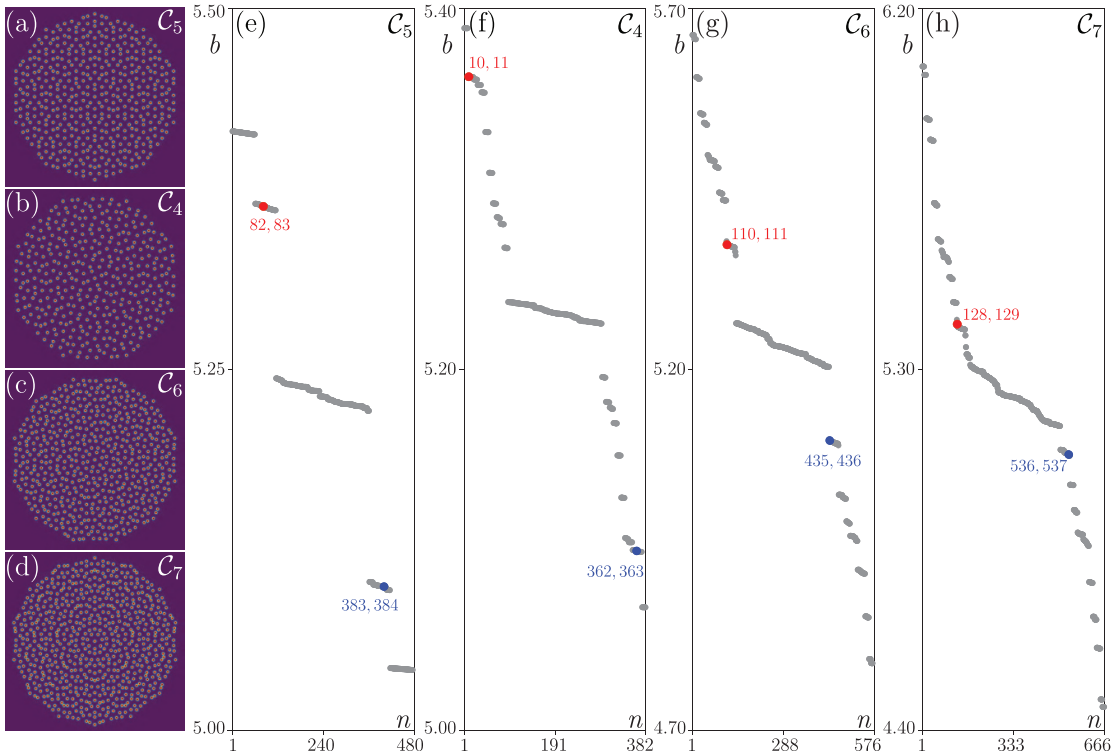

Figure 2. Disclination quasicrystalline lattices and their spectra. (a) Quasicrystal generated using Penrose tiling and its linear spectrum in the form of dependence of eigenvalues of all modes b on mode index n (e). (b) $\mathcal{C}_4$ symmetric disclination quasicrystal and its spectrum (f). (c) $\mathcal{C}_6$ symmetric disclination quasicrystal and its spectrum (g). (d) $\mathcal{C}_7$ symmetric disclination quasicrystal and its spectrum (h). Colored dots in (e)–(h) represent the pairs of degenerate states, whose linear combination produces vortices with $m \pm 1$.

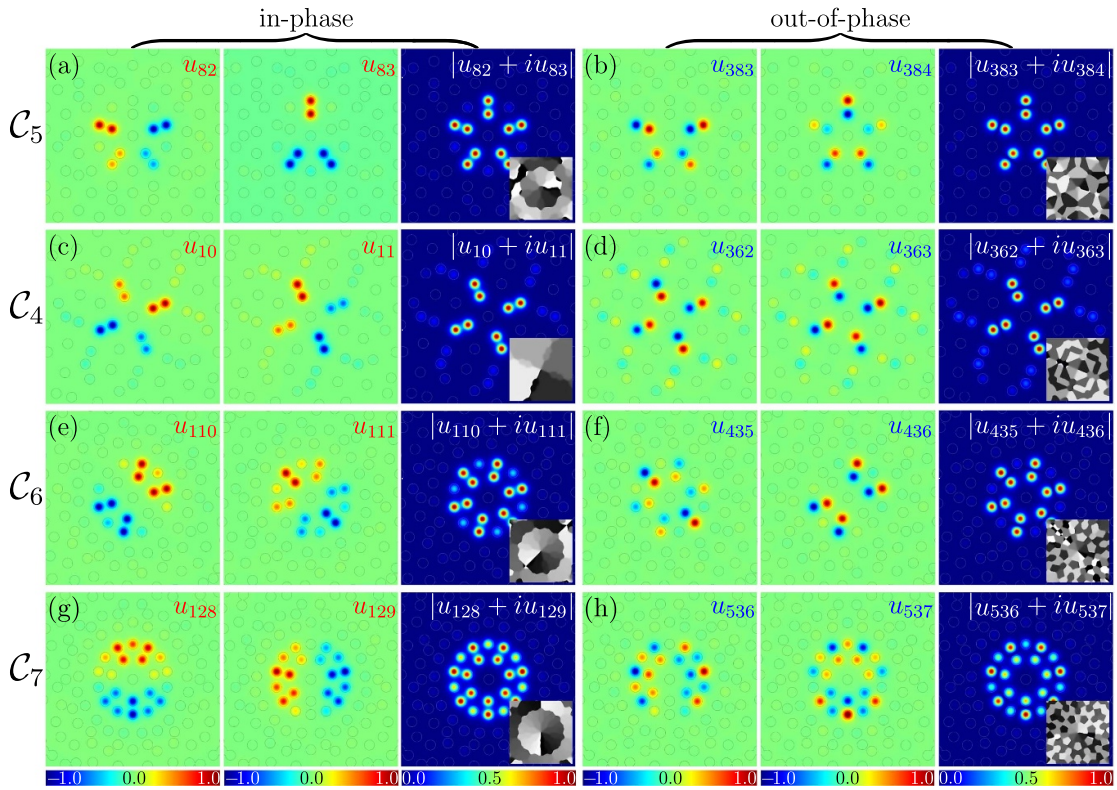

Figure 3. Vortex state with $m = \pm 1$ comprising degenerate modes. (a) Profiles of two degenerate modes u_{82} and u_{83}, and modulus and phase (inset) distributions in the in-phase vortex state $u_{82} + iu_{83}$ constructed using these modes in the $\mathcal{C}_5$ quasicrystal corresponding to Penrose tiling. (b) Degenerate modes u_{383} and u_{384} and out-of-phase vortex supported by $\mathcal{C}_5$ quasicrystal. Other panels depict the profiles of degenerate modes and in-phase and out-of-phase vortices constructed on them in $\mathcal{C}_4$ (c), (d), $\mathcal{C}_6$ (e), (f), and $\mathcal{C}_7$ (g), (h) disclination quasicrystals. For the convenience of presentation and comparison of different modes, the peak amplitude of each linear mode in this figure is normalized to 1. The faint circles in each panel represent the lattice sites. Profiles are shown within the window $-10 \leqslant x, y \leqslant 10$.

the eigenvalue problem $bu = (1/2)\nabla^2 u + \mathcal{R}u$ that can be obtained from equation (1) and solved using the plane-wave expansion method.

The linear spectrum of 'parent' $\mathcal{C}_5$ Penrose quasicrystal with selected tiling in the form of dependence of propagation constant $b = b_n$ (sorted such that modes with lower indices have higher propagation constants) on mode index n is presented in figure 2(e). One can see that propagation constants are organized in five minibands. Among them, the modes with indices $n = 82, 83$ (red dots) and $n = 383, 384$ (blue dots) are localized at the very center of the quasicrystal and form degenerate pairs. Profiles of modes $n = 82, 83$ are depicted in figure 3(a), whereas those of modes $n = 383, 384$ are shown in figure 3(b). Closely located pairs of spots in the profiles of these modes are respectively in-phase and out-of-phase. The coexistence of two such types of localized modes close to the center of the quasicrystal is a result of the selected Penrose tiling. Linear combinations of these modes $u_{82} \pm \mathrm{i}u_{83}$ and $u_{383} \pm \mathrm{i}u_{384}$ produce vortex-carrying states with topological charges $m = \pm 1$, whose modulus and phase distributions are illustrated in figures 3(a) and (b). Notice distinctly different phases of these states: the phase of the vortex produced by out-of-phase states is strongly radially modulated, compared to the phase of the vortex produced by in-phase states. So-constructed *in-phase* and *out-of-phase* vortices can propagate without variations in their shapes in $\mathcal{C}_5$ quasicrystal, and to the best of our knowledge, they have never been reported before. Among the surprising properties of vortex states is their pronounced localization despite the fact that their propagation constants are located in spectral mini-bands. This is a consequence of the sufficiently large depth p of waveguides considered here, which ensures that we work in a regime well above delocalization-localization transition in $\mathcal{C}_5$ quasicrystal. According to our simulations, degenerate localized modes that would have equal propagation constants and that would be able to produce vortical states localized at the off-center positions in quasicrystal lattices are absent in the linear spectrum.

The introduction of a global deformation that results in the formation of $\mathcal{C}_4$ quasicrystal with disclination results in a substantial modification of the linear spectrum (figure 2(f)), where one observes the formation of multiple mini-bands with close propagation constants. This is because the introduction of disclination changes the interwaveguide spacing differently at different distances from the center of the

quasicrystal, and instead of only two characteristic nearest-neighbor spacing values (as in $\mathcal{C}_5$ quasicrystal), one now obtains a structure with multiple nearest-neighbor spacings. Still, two pairs of degenerate modes localized near the center of $\mathcal{C}_4$ quasicrystal are found in the linear spectrum in figure 2(f), whose linear combinations produce in-phase and out-of-phase vortex states depicted in figures 3(c) and (d). Linear spectra of $\mathcal{C}_6$ and $\mathcal{C}_7$ disclination quasicrystals displayed in figures 2(g) and (h), respectively, show similar fractionalization, but in all cases, it is possible to construct stationary vortex-carrying states residing in the centers of the corresponding quasicrystals (see modulus and phase distributions in figures 3(e)–(h)) that feature the same discrete rotational symmetry as that of the quasicrystal. The introduction of disclination therefore appears as a powerful tool allowing the construction of spatially localized vortex states with a desired symmetry. It should be stressed that while we concentrate here on linear combinations producing $m = \pm 1$ vortices, other groups of degenerate modes exist in the system's linear spectrum that allow the construction of vortices with higher charges permitted by the discrete rotational symmetry of the quasicrystal [28, 29]. Therefore, $\mathcal{C}_5$ and $\mathcal{C}_6$ quasicrystals with disclinations allow the construction of vortex states with topological charges up to $m = \pm 2$, whereas $\mathcal{C}_7$ quasicrystals allow the construction of vortex states with charges up to $m = \pm 3$, which are displayed in **supplemental materials**. Note that the maximal value of the topological charge of the vortex that can be supported by the quasicrystal with disclination can be predicted using the arguments of group theory, see details in [28, 29]. Thus, in $\mathcal{C}_4$ structures, only the topological charges $m = \pm 1$ are compatible with the discrete rotational symmetry of the lattice, whereas vortex states with $|m| \geqslant 2$ are forbidden as irreducible representations of the $\mathcal{C}_4$ group. The linear spectrum of the corresponding quasicrystals directly reflects this property since discrete rotational symmetry $\mathcal{C}_k$ determines the number of pairs of localized degenerate states (producing vortices) that can be found in the entire spectrum. In each case, for a given charge m, it is possible to construct both in-phase and out-of-phase types of vortices (by analogy with the results shown in figure 3), by using a combination of proper linear modes. Furthermore, as the order of the discrete rotational symmetry increases, the formation of vortex states with even higher charges can be expected. Therefore, the ability to alter discrete rotational symmetry renders disclination quasicrystals a versatile platform for the generation of vortices with tailored charges that remain spatially localized in these aperiodic systems above delocalization-localization transition (above a certain threshold value of p).

2.3. Vortex solitons and stability analysis

In this section, we obtain vortex soliton families bifurcating from the above linear localized vortex states. The profiles of such vortex solitons can be found from the equation $bu = (1/2)\nabla^2 u + \mathcal{R}u + |u|^2 u$, where we account for the focusing nonlinearity of the material, and where the function u describing the soliton profile is now complex and determined by the propagation constant b, which is now a free parameter. We solve this equation using the Newton method. We primarily concentrate here on vortex soliton families originating from out-of-phase linear vortex states, but their in-phase counterparts can be analyzed using a similar approach.

Out-of-phase vortex soliton families with $|m| = 1$ in Penrose quasicrystal with $\mathcal{C}_5$ discrete rotational symmetry are presented in figure 4(a) by the dependence of soliton power $U = \iint |u|^2 \mathrm{d}x\mathrm{d}y$ on the propagation constant b. As the nonlinearity of the medium is focused, bifurcation from the linear vortex occurs in the direction of increasing b. When soliton propagation constant b approaches the eigenvalue $b_{n=383,384}$ of degenerate linear modes that produce an out-of-phase vortex, both amplitude $\max|u|$ and power U of soliton vanish, that is, such states are thresholdless for our parameters (see blue line in figure 4(a)) compared to all previously reported vortex solitons in quasicrystals. When the propagation constant b of vortex soliton crosses the mini-bands (represented by gray regions in figure 4(a)), the coupling between different modes belonging to this mini-band unavoidably occurs and this leads to substantial shape transformation and overall expansion of the vortex soliton (because modes from mini-bands can be concentrated at different spatial locations inside the quasicrystal). Since coupling may occur with multiple modes that renders $U(b)$ dependence very complicated and yields the coexistence of many different types of vortical solutions, we do not trace it inside mini-bands. The family of well-localized out-of-phase vortex solitons residing in the center of the quasicrystal can be continued to other spectral gaps, both finite (green line) and semiinfinite (orange line) ones, as shown in figure 4(a). Notice that the internal structure of vortex solitons with representative π phase difference between spots in close pairs is maintained also in higher gaps, but the overall phase distribution gradually simplifies (the number of phase jumps in the radial direction decreases in higher gaps as one can see from the insets in figure 4(e) with soliton profiles). Therefore, nonlinearity provides a powerful knob to control localization, internal and phase structure of vortex excitations in aperiodic materials.

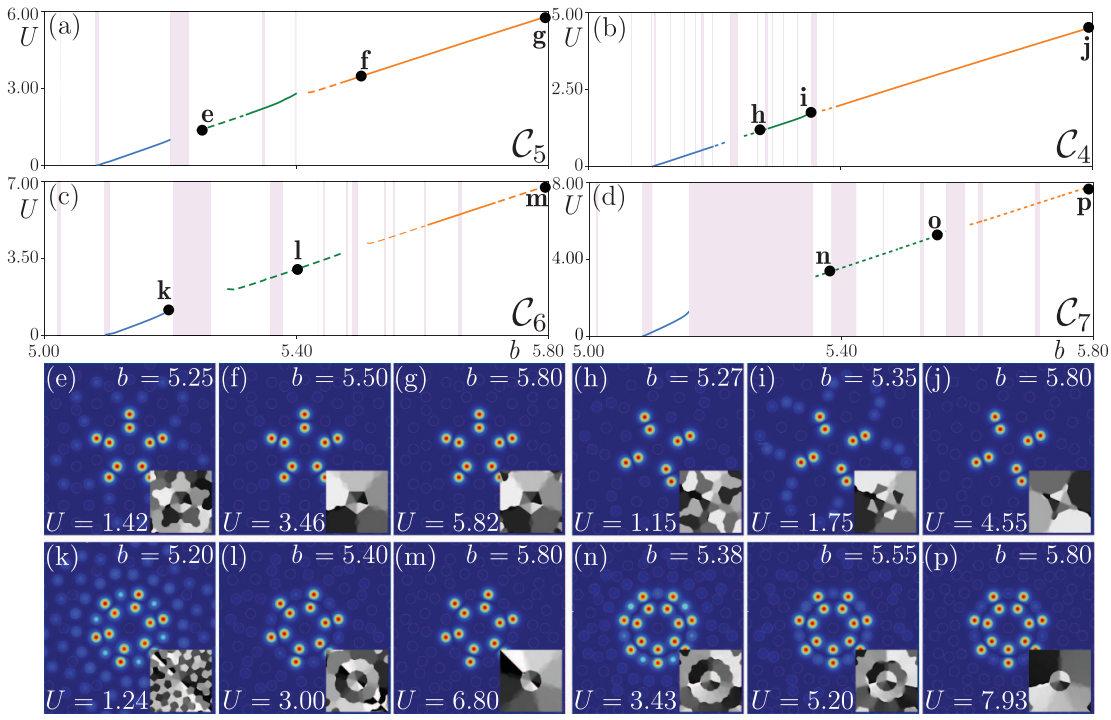

Figure 4. Vortex soliton families with $m = \pm 1$. (a)–(d) $U(b)$ dependencies for out-of-phase vortex soliton families with topological charge $|m| = 1$ in quasicrystals with different discrete rotational symmetries. Gray areas correspond to mini-bands from linear spectra in figure 2. (e)–(p) Field modulus and corresponding phase (insets) distributions of the vortex solitons corresponding to the dots with letters in $U(b)$ dependencies.

The families of out-of-phase vortex solitons in $\mathcal{C}_4$, $\mathcal{C}_6$, and $\mathcal{C}_7$ quasicrystals with disclinations are presented in figures 4(b)–(d), respectively. Since the complexity of the linear spectrum substantially increases upon the introduction of disclination into the quasicrystal, resulting in the appearance of multiple mini-bands in the spectrum (in comparison with only five mini-bands in Penrose $\mathcal{C}_5$ case), vortex solitons cross such multiple mini-bands upon an increase in propagation constant b. Still, coupling occurs only with a selected small subset of mini-bands (since for some mini-bands, it is prohibited by different symmetry, or by very different locations of the vortex soliton and linear states of this mini-band). As a result, it is possible to trace $U(b)$ families in wide power ranges, as shown in figures 4(b)–(d). It should be mentioned that in real experimental conditions, when vortex states are excited by localized inputs with designed phase distributions, one would observe namely such transitions between soliton families from different spectral gaps upon an increase in the input power (provided that the corresponding solitons are stable), perhaps accompanied by spreading in narrow power intervals, where coupling with other modes can occur. Representative field modulus and phase distributions of out-of-phase vortex solitons in $\mathcal{C}_4$, $\mathcal{C}_6$, and $\mathcal{C}_7$ quasicrystals are depicted in figures 4(h)–(p). One can see how the discrete rotational symmetry of the intensity distribution of the vortex soliton increases with increasing lattice symmetry. For some profiles taken sufficiently close to mini-bands (see dots in corresponding $U(b)$ dependencies), one can see broadening of solitons due to coupling with linear modes at other spatial locations. Just as in $\mathcal{C}_5$ case, the tendency toward the simplification of the phase distribution is visible in higher spectral gaps.

The stability of solitons represents one of the most fundamental and crucial prerequisites for their potential experimental observation. We use a two-fold approach to the characterization of stability of the obtained families: linear stability analysis and direct propagation of the perturbed states, allowing us to assess stability beyond the perturbative approach, even when the actual perturbations are not small. In the latter case, we add random noise into the input vortex solitons with amplitude up to 10% of soliton's peak amplitude, and propagate them over long distance $z \sim 8000$. A perturbed soliton is considered stable if it retains its integrity and characteristic phase structure throughout propagation; otherwise, it is classified as unstable. According to this method, the largest part of the out-of-phase vortex soliton families in $\mathcal{C}_4$ and $\mathcal{C}_5$ quasicrystals corresponding to solid lines in figures 4(a) and (b) is stable. Instabilities are encountered only in narrow ranges of b values (see dashed lines in figures 4(a) and (b)), typically, close to mini-bands. Notably, as the discrete rotational symmetry order of the system increases,

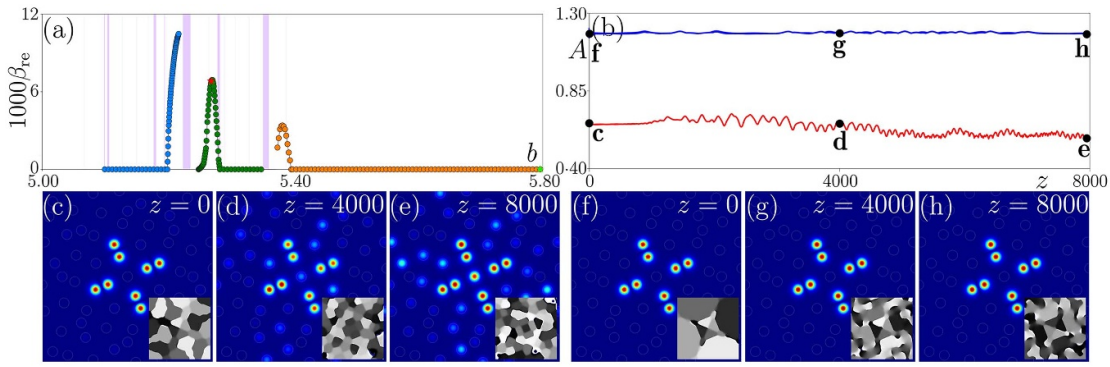

Figure 5. Linear stability analysis of vortex solitons in the $\mathcal{C}_4$ quasicrystal. (a) Perturbation growth rate $\beta_{\rm re}$ versus propagation constant b for out-of-phase vortex solitons in $\mathcal{C}_4$ quasicrystal. (b) Peak amplitude $A = \max|\psi|$ of representative stable (blue curve) and unstable (red curve) perturbed vortex solitons versus propagation distance. (c)–(h) Field modulus phase distributions of solitons at different propagation distances corresponding to the dots in panel (b).

the instability domains broaden - see dashed parts of the soliton families in figures 4(c) and (d) corresponding to $\mathcal{C}_6$ and $\mathcal{C}_7$ quasicrystals. In all cases, vortex solitons are metastable near bifurcation points of linear vortex modes.

To complete the above analysis, we also performed a linear stability analysis that requires superimposing small perturbations w and v onto the vortex soliton profile u as follows:

$$\psi = \left[u(x,y) + v(x,y)\, e^{\beta z} + w^*(x,y)\, \mathrm{e}^{\beta^* z}\right] \mathrm{e}^{\mathrm{i}bz} \tag{3}$$

where $v, w \ll u$, and $\beta = \beta_{\rm re} + \mathrm{i}\beta_{\rm im}$ is the complex perturbation growth rate. Substituting equation (3) into equation (1) and linearizing the resulting equation around the stationary solution u, one arrives at the following linear eigenvalue problem:

$$\begin{aligned} \mathrm{i}\beta v &= -\frac{1}{2}\nabla^2 v - (\mathcal{R} - b)\, v - 2|u|^2 v - |u|^2 w, \\ \mathrm{i}\beta w &= +\frac{1}{2}\nabla^2 w + (\mathcal{R} - b)\, w + 2|u|^2 w + |u|^2 v. \end{aligned} \tag{4}$$

Solving the problem (4) using standard eigenvalue solver, we obtain the dependence of the perturbation growth rate β (and associated perturbation profiles v, w) on the propagation constant b for a given family of vortex solitons. A vortex soliton u is deemed linearly stable if the real part of the perturbation growth rate $\beta_{\rm re} \leqslant 0$ for all possible perturbations; in this case, the soliton will only exhibit small-amplitude oscillations during propagation even in the presence of small perturbations. In contrast, if at least one perturbation mode yields $\beta_{\rm re} > 0$, the vortex soliton is unstable, and it will decay as it propagates. In figure 5(a), we show the maximal real part of the perturbation growth rate $\beta_{\rm re}(b)$ for the vortex soliton families in the $\mathcal{C}_4$ quasicrystal, as a representative example. Notably, the linear stability analysis results are in excellent agreement with those obtained via the direct propagation of perturbed states (cf dashed lines in figure 4(b)). Red and green stars in figure 5(a) correspond to, respectively, unstable and stable states h and i in figure 4(b). Peak amplitudes of these perturbed states during propagation are shown in figure 5(b), whereas field modulus and phase distributions at different distances are shown in figures 5(c)–(e). The unstable state loses its vorticity and displays considerable amplitude oscillations upon propagation due to tunneling of power into other sites of the quasicrystal (red curve), whereas the stable state keeps its internal structure and shows minimal oscillations (blue curve).

As mentioned above, disclination quasicrystals also support rich families of in-phase vortex solitons. These solitons demonstrate very interesting nonlinear transformations upon increase in power, when different branches of solutions can bifurcate from a given family (bifurcating from a linear in-phase vortex state), characterized by equal intensities of spots in close pairs (see left outermost solutions in figure 6). With an increase in the propagation constant b, two branches of solutions emerge in one of which light concentrates on outer sites from close pairs, as in figures 6(a), (c), (e) and (g), whereas in solutions belonging to the other branch, light concentrates on inner sites from close pairs, as in figures 6(b), (d), (f) and (h). This is the result of a classical symmetry-breaking bifurcation in the focusing medium that

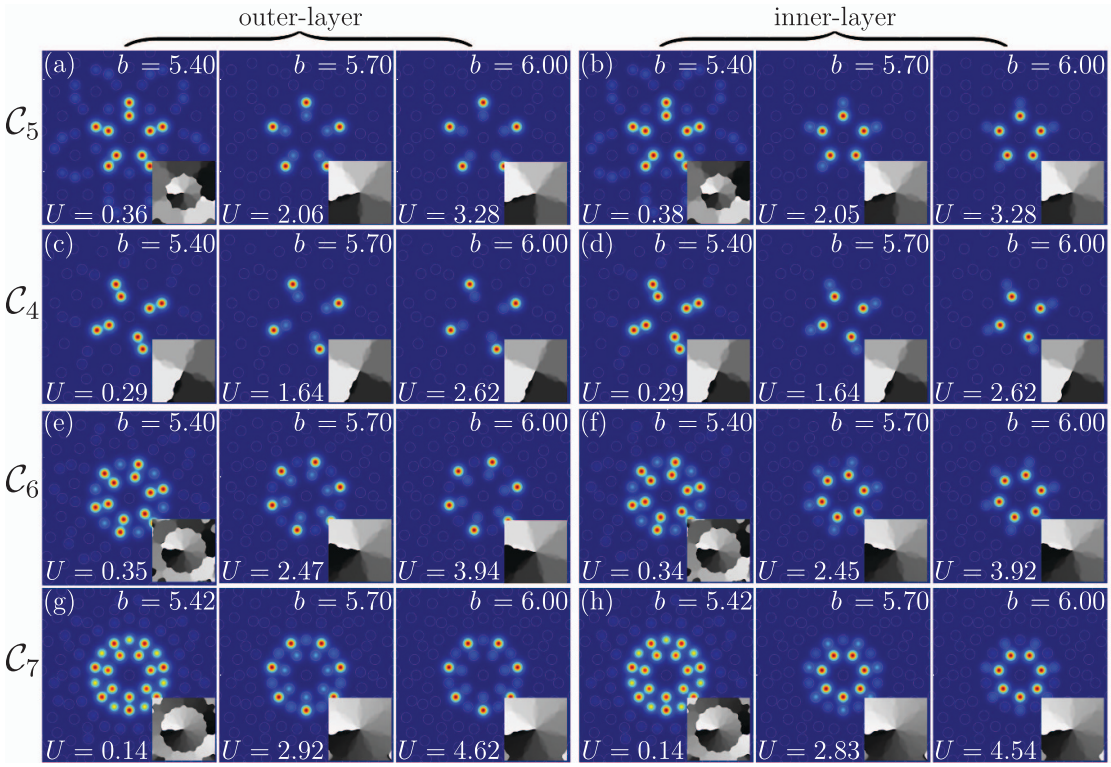

Figure 6. Field modulus and phase (insets) distributions for $m = \pm 1$ in-phase vortex solitons illustrating their rich shape transformations with increase of propagation constant b in (a), (b) original Penrose quasicrystal with $\mathcal{C}_5$ symmetry, and quasicrystals with disclinations with (c), (d) $\mathcal{C}_4$, (e), (f) $\mathcal{C}_6$, and (g), (h) $\mathcal{C}_7$ symmetry. Parameters of quasicrystals are the same as in figure 2.

doubles the number of possible in-phase solutions for a given spectral gap (we do not show here corresponding $U(b)$ dependencies due to their complexity). Such bifurcations occur for all types of quasicrystals considered here. Just like in out-of-phase solitons, the intensity distributions of in-phase solitons reflect the discrete rotational symmetry of the corresponding quasicrystal. The coexistence of two different types of in-phase and out-of-phase vortex solitons in quasicrystals is a result of their rich and aperiodic spatial structure determined by the 'parent' Penrose tiling.

In the above analysis we concentrate only on vortex soliton families with topological charge $|m| = 1$. In supplemental materials, we provide other examples of degenerate eigenmodes, whose linear combinations can produce vortices with higher topological charges $|m| > 1$ (in particular, in $\mathcal{C}_6$ and $\mathcal{C}_7$ quasicrystals). All such linear vortex modes give rise to families of thresholdless vortex solitons. Our simulations demonstrate that vortex solitons with different topological charges emerging from different linear modes may coexist within some gaps. Still, vortex solitons with different topological charges do not couple because they are orthogonal (due to different charges), that is, their overlap integral is zero even in the nonlinear case.

3. Discussions

3.1. Approximations and limitations

Before closing, we would like to stress that the approach to the creation of quasicrystals with disclinations suggested here is powerful and leads to multiple unusual thresholdless vortex states, but it is, of course, not free from certain limitations.

First, one has to consider that increasing the discrete rotational symmetry of the quasicrystal structure due to the addition of sectors with larger and larger Franck angles leads to a gradual increase in the density of waveguides and sooner or later they will start overlapping. This may qualitatively affect the linear spectrum of the system and, besides possible technological difficulties in the creation of such structures with tightly packed waveguides, this imposes natural limitations on the maximal order of discrete rotational symmetry that can be realized with this approach. Likewise, removing too large Franck angles will result in quasicrystal structures with too sparse arrangement of practically noninteracting waveguides (that would be reflected in very narrow spectral bands).

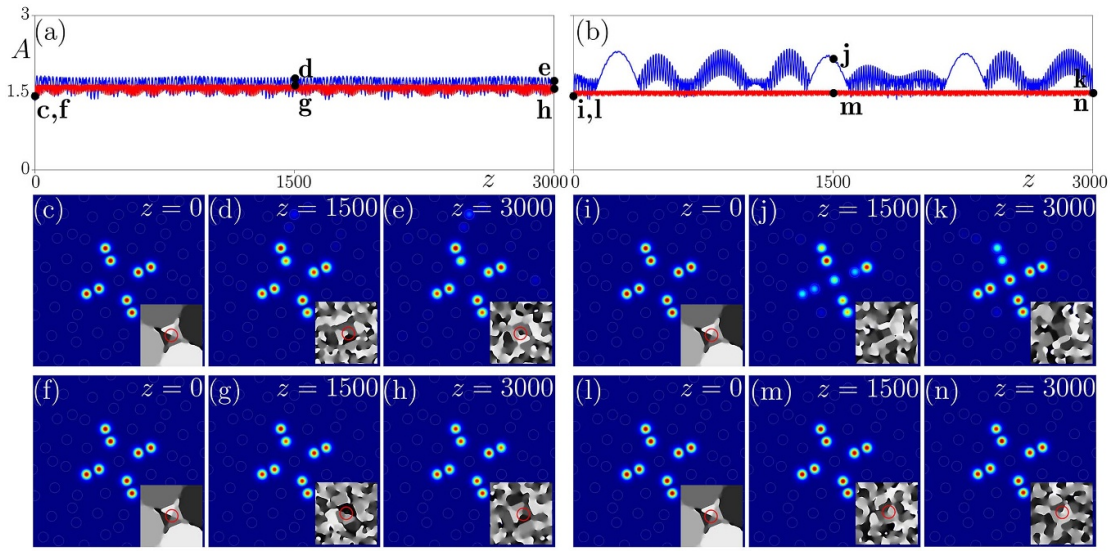

Figure 7. Peak amplitude of the vortex state upon propagation in $\mathcal{C}_4$ quasicrystal with 3% (a) and 6% (b) positional and depth disorder. Blue and red curves correspond to linear propagation and nonlinear propagation, respectively. (c)–(h) Field modulus and phase distributions corresponding to dots in (a). (i)–(n) Field modulus and phase distributions corresponding to dots in (b). Red circles highlight phase singularity in the center of the pattern.

The second limitation is connected with the fact that the original $\mathcal{C}_5$ structure produced by the Penrose tiling of the plane that we use as a platform for the construction of disclination arrays is not unique. Hence, the selection of other tilings may produce disclination quasicrystals with different spectral features. They will still support vortex states with topological charges predicted by our analysis, but the details of the modal shapes may be different, leading to different nonlinear families and bifurcations.

Finally, it should be mentioned that our results and methods are applicable for structures with shallow transverse refractive index modulation and for paraxial light beams. At the same time, these ideas can be potentially extended to nonparaxial models and nanoscale quasicrystalline devices using the full-wave analysis [76].

3.2. Influence of disorder on vortex states in quasicrystals

The robustness of vortex solitons in quasicrystals with respect to perturbations of initial waveforms ψ has been studied by us in section 2.3. However, under realistic experimental conditions, a certain level of disorder/imperfection may be present in the underlying optical potential landscape $\mathcal{R}$ breakings its ideal $\mathcal{C}_\nu$ discrete rotational symmetry. In this section, we consider the impact of such disorder on the propagation dynamics of vortex states in both linear and nonlinear regimes. To this end, we introduce both diagonal (depth) and off-diagonal (position) disorder into the underlying lattice (2) by letting the depths of individual waveguides in the lattice to fluctuate (uniform distribution) within the range $[p(1-\delta_p), p(1+\delta_p)]$, whereas deviations of positions of waveguide centers $(x_{m,n}, y_{m,n})$ from their regular values are allowed to vary within the interval $[a(1-\delta_a), a(1+\delta_a)]$. We gradually increase the strength of disorder characterized by parameters δ_p, δ_a taking for simplicity $\delta_p = \delta_a$ and consider its impact on the evolution of vortex modes in the linear and nonlinear regimes. We consider different realizations of disorder with strength up to 10%. Modern fs-laser writing technology usually allows to achieve much better accuracy of positioning (at the level of several nanometers for typical spacings of tens of micrometers) and uniformity of waveguide depths across the structure (especially when multitrack writing technology is employed [67]). Typical scenarios of propagation of vortices in exemplary $\mathcal{C}_4$ structure with disorder are presented in figure 7. The presence of weak disorder (3% in this case) in the underlying structure causes oscillations of the peak amplitude A of vortex state during propagation that are stronger in the linear case (blue curve) compared to the nonlinear case (red curve) (figure 7(a)). Although disorder causes slight shape transformations of the input state and may result in a slight displacement of the phase singularity from the center of the lattice (see representative modulus and phase (insets) distributions in figures 7(c)–(e) for a linear case, and in figures 7(f)–(h) for a nonlinear case), the primary outcome of the analysis is that it withstands the presence of weak disorders in the underlying lattice. This conclusion holds for disorder levels up to approximately 4%. When the strength of disorder is increased to approximately 6%, multiple disorder realizations appear where the initial vortex-carrying state exhibits

considerable shape transformations in the linear case (the spots in the vortex profile change their intensities, coupling with other modes is possible that leads to an overall expansion of the propagating field, and vorticity in the center of the structure is lost), the example is shown in figures 7(i)–(k). Such transformations are usually accompanied by considerable amplitude oscillations (figure 7(b)). However, when the same input vortex state propagates in a nonlinear medium, nonlinearity may play a strong stabilizing action, even in the presence of disorder. In this case, the amplitudes of the spots in the vortex profile become nearly equal in amplitude, the amplitude oscillations are suppressed, and vorticity is clearly preserved, as shown in figures 7(l)–(n). Such behavior has been observed for the majority of disorder realizations. These findings confirm that vortex modes are experimentally observable in quasicrystals with disclinations.

4. Conclusion

In conclusion, we have investigated the formation of vortex solitons in quasicrystals by introducing into them a global topological deformation resulting in the formation of disclination structures with variable discrete rotational symmetry. Starting from 'parent' C_5 Penrose tiling, we obtain various aperiodic disclination lattices with $C_{4,6,7}$ discrete rotational symmetry. Despite considerable fractionalization of the spectrum due to the introduction of disclination, each of these quasicrystals support sets of localized (above delocalization-localization transition threshold) degenerate states in the center of the structure that can produce in-phase and out-of-phase vortices with topological charges limited by the discrete rotational symmetry of the underlying structure. We also encounter rich families of in-phase and out-of-phase vortex solitons bifurcating from such linear vortical states and existing across a wide range of powers. The localization, intensity and phase structure of such states is controlled by their power in a nonlinear medium, thereby illustrating that nonlinearity may serve as a convenient tool for controlling the structure of propagating light beams in such aperiodic materials with long-range order. Our results may be useful for the design of novel switching and transmission devices for states carrying nonzero orbital angular momentum, as well as for new classes of lasers and quantum memories harnessing new types of discrete rotational symmetries of aperiodic refractive index landscapes.

The results obtained here can also be generalized to the case of quasicrystals with defocusing nonlinearity following the method utilized in this work. Such states would bifurcate from linear vortex modes in the direction of decreasing propagation constants. Preliminary analysis demonstrates that vortex solitons in a defocusing medium demonstrate exceptional stability and resilience to disorder.

Acknowledgments

This work was supported by the National Natural Science Foundation of China (Grant Nos. 12304370 and 12474337), the Natural Science Basic Research Program of Shaanxi Province (Grant Nos. 2024JC-JCQN-06 and 2025JC-QYCX-006), the Key Research and Development Program of Shaanxi Province (Grant No. 2025CY-YBXM-037), the Postdoctoral Research Project of Shaanxi Province (Grant No. 2023BSHYDZZ14), the Sichuan Science and Technology Program (Grant No. 2025ZNSFSC1458), the Fundamental Research Funds for the Central Universities (Grant No. xzy012024135), the Russian Science Foundation (Grant No. 24-12-00167), and partially by the project FFUU-2024-0003 of the Institute of Spectroscopy of Russian Academy of Sciences.

Data availability statement

The data cannot be made publicly available upon publication because they are not available in a format that is sufficiently accessible or reusable by other researchers. The data that support the findings of this study are available upon reasonable request from the authors.

Supplementary data 1 available at https://doi.org/10.1088/1361-6633/ae73b5/data1.

Conflict of interest

The authors declare no competing interests.

Author contributions

Hua Zhong 0009-0008-3057-9574
Data curation (equal), Formal analysis (equal), Funding acquisition (equal), Investigation (lead), Writing – original draft (equal), Writing – review & editing (equal)

Yaroslav V Kartashov 0000-0001-8692-982X
Conceptualization (equal), Data curation (equal), Formal analysis (equal), Investigation (equal), Supervision (equal), Writing – original draft (equal), Writing – review & editing (equal)

Yongdong Li 0000-0001-8756-0438
Supervision (equal), Writing – original draft (equal), Writing – review & editing (equal)

Fangwei Ye 0000-0003-2263-9000
Supervision (equal), Writing – original draft (equal), Writing – review & editing (equal)

Yiqi Zhang 0000-0002-5715-2182
Conceptualization (lead), Data curation (lead), Formal analysis (lead), Funding acquisition (lead), Investigation (equal), Supervision (lead), Writing – original draft (lead), Writing – review & editing (lead)

References

[1] Georgescu I 2024 50 years of Penrose tilings *Nat. Rev. Phys.* **6** 408
[2] Shechtman D, Blech I, Gratias D and Cahn J W 1984 Metallic phase with long-range orientational order and no translational symmetry *Phys. Rev. Lett.* **53** 1951–3
[3] Levine D and Steinhardt P J 1984 Quasicrystals: a new class of ordered structures *Phys. Rev. Lett.* **53** 2477–80
[4] Guyot P, Kramer P and de Boissieu M 1991 Quasicrystals *Rep. Prog. Phys.* **54** 1373
[5] Steurer W 2018 Quasicrystals: what do we know? What do we want to know? What can we know? *Acta. Crystallogr. A.* **74** 1–11
[6] Lifshitz R 1998 Symmetry of magnetically ordered quasicrystals *Phys. Rev. Lett.* **80** 2717–20
[7] Vedmedenko E Y, Grimm U and Wiesendanger R 2004 Noncollinear magnetic order in quasicrystals *Phys. Rev. Lett.* **93** 076407
[8] Tamura R *et al* 2025 Observation of antiferromagnetic order in a quasicrystal *Nat. Phys.* **21** 974–9
[9] Viebahn K, Sbroscia M, Carter E, Yu J C and Schneider U 2019 Matter-wave diffraction from a quasicrystalline optical lattice *Phys. Rev. Lett.* **122** 110404
[10] Vardeny Z V, Nahata A and Agrawal A 2013 Optics of photonic quasicrystals *Nat. Photon.* **7** 177–87
[11] Freedman B, Bartal G, Segev M, Lifshitz R, Christodoulides D N and Fleischer J W 2006 Wave and defect dynamics in nonlinear photonic quasicrystals *Nature* **440** 1166–9
[12] Freedman B, Lifshitz R, Fleischer J W and Segev M 2007 Phason dynamics in nonlinear photonic quasicrystals *Nat. Mater.* **6** 776–81
[13] Levi L, Rechtsman M, Freedman B, Schwartz T, Manela O and Segev M 2011 Disorder-enhanced transport in photonic quasicrystals *Science* **332** 1541–4
[14] Bandres M A, Rechtsman M C and Segev M 2016 Topological photonic quasicrystals: Fractal topological spectrum and protected transport *Phys. Rev. X* **6** 011016
[15] Wang P, Fu Q, Konotop V V, Kartashov Y V and Ye F 2024 Observation of localization of light in linear photonic quasicrystals with diverse rotational symmetries *Nat. Photon.* **18** 224–9
[16] Xu C, Zhao R, Zhang X, Zhang S, Li X, Geng G, Li J, Li X, Wang Y and Huang L 2024 Quasicrystal metasurface for dual functionality of holography and diffraction generation *eLight* **4** 9
[17] Ivanov S K *et al* 2025 Observation of light localization at the edges of quasicrystal waveguide arrays *Phys. Rev. Lett.* **134** 113803
[18] Zhang Y, Lan Z, Hu L, Shu Y, Yuan X, Guo P, Peng X, Chen W and Li J 2023 Chiral photonic topological states in Penrose quasicrystals *Opt. Lett.* **48** 2229–32
[19] de Espinosa F M, Torres M, Pastor G, Muriel M A and Mackay A L 1993 Acoustic quasi-crystals *Europhys. Lett.* **21** 915
[20] Han C, Chen L Q, Yang T, Xu G, Li J, Li C, Fan H, Alú A and Qiu C W 2025 Observation of dispersive acoustic quasicrystals *Nat. Commun.* **16** 1988
[21] Wang P, Zheng Y, Chen X, Huang C, Kartashov Y V, Torner L, Konotop V V and Ye F 2020 Localization and delocalization of light in photonic moiré lattices *Nature* **577** 42–46
[22] Fu Q, Wang P, Huang C, Kartashov Y V, Torner L, Konotop V V and Ye F 2020 Optical soliton formation controlled by angle twisting in photonic moiré lattices *Nat. Photon.* **14** 663–8
[23] Meng Z, Wang L, Han W, Liu F, Wen K, Gao C, Wang P, Chin C and Zhang J 2023 Atomic Bose-Einstein condensate in twisted-bilayer optical lattices *Nature* **615** 231–6
[24] Du L, Molas M R, Huang Z, Zhang G, Wang F and Sun Z 2023 Moiré photonics and optoelectronics *Science* **379** eadg0014
[25] Lahini Y, Avidan A, Pozzi F, Sorel M, Morandotti R, Christodoulides D N and Silberberg Y 2008 Anderson localization and nonlinearity in one-dimensional disordered photonic lattices *Phys. Rev. Lett.* **100** 013906
[26] Shen Y, Wang X, Xie Z, Min C, Fu X, Liu Q, Gong M and Yuan X 2019 Optical vortices 30 years on: OAM manipulation from topological charge to multiple singularities *Light Sci. Appl.* **8** 90
[27] Chen S *et al* 2025 Optical vortices in communication systems: mode (de)modulation, processing and transmission *Adv. Photon.* **7** 044001
[28] Ferrando A, Zacarés M and García-March M A 2005 Vorticity cutoff in nonlinear photonic crystals *Phys. Rev. Lett.* **95** 043901
[29] Kartashov Y V, Ferrando A, Egorov A A and Torner L 2005 Soliton topology versus discrete symmetry in optical lattices *Phys. Rev. Lett.* **95** 123902

[30] Dong L, Kartashov Y V, Torner L and Ferrando A 2022 Vortex solitons in twisted circular waveguide arrays *Phys. Rev. Lett.* **129** 123903
[31] Malomed B A and Kevrekidis P G 2001 Discrete vortex solitons *Phys. Rev. E* **64** 026601
[32] Neshev D N, Alexander T J, Ostrovskaya E A, Kivshar Y S, Martin H, Makasyuk I and Chen Z 2004 Observation of discrete vortex solitons in optically induced photonic lattices *Phys. Rev. Lett.* **92** 123903
[33] Fleischer J W, Bartal G, Cohen O, Manela O, Segev M, Hudock J and Christodoulides D N 2004 Observation of vortex-ring 'discrete' solitons in 2D photonic lattices *Phys. Rev. Lett.* **92** 123904
[34] Terhalle B, Richter T, Desyatnikov A S, Neshev D N, Krolikowski W, Kaiser F, Denz C and Kivshar Y S 2008 Observation of multivortex solitons in photonic lattices *Phys. Rev. Lett.* **101** 013903
[35] Terhalle B *et al* 2009 Observation of double-charge discrete vortex solitons in hexagonal photonic lattices *Phys. Rev. A* **79** 043821
[36] Desyatnikov A S, Kivshar Y S and Torner L 2005 Optical vortices and vortex solitons *Prog. Opt.* **47** 291–391
[37] Lederer F, Stegeman G I, Christodoulides D N, Assanto G, Segev M and Silberberg Y 2008 Discrete solitons in optics *Phys. Rep.* **463** 1–126
[38] Kartashov Y V, Malomed B A and Torner L 2011 Solitons in nonlinear lattices *Rev. Mod. Phys.* **83** 247–305
[39] Kartashov Y V, Astrakharchik G E, Malomed B A and Torner L 2019 Frontiers in multidimensional self-trapping of nonlinear fields and matter *Nat. Rev. Phys.* **1** 185–97
[40] Mihalache D 2017 Multidimensional localized structures in optical and matter-wave media: A topical survey of recent literature *Rom. Rep. Phys.* **69** 403
[41] Malomed B A 2019 Vortex solitons: old results and new perspectives *Physica D* **399** 108–37
[42] Pryamikov A, Hadzievski L, Fedoruk M, Turitsyn S and Aceves A 2021 Optical vortices in waveguides with discrete and continuous rotational symmetry *J. Eur. Opt. Soc.-Rapid Publ.* **17** 23
[43] Xie P, Zhang Z Q and Zhang X 2003 Gap solitons and soliton trains in finite-sized two-dimensional periodic and quasiperiodic photonic crystals *Phys. Rev. E* **67** 026607
[44] Sakaguchi H and Malomed B A 2006 Gap solitons in quasiperiodic optical lattices *Phys. Rev. E* **74** 026601
[45] Ablowitz M J, Ilan B, Schonbrun E and Piestun R 2006 Solitons in two-dimensional lattices possessing defects, dislocations and quasicrystal structures *Phys. Rev. E* **74** 035601
[46] Law K J H, Saxena A, Kevrekidis P G and Bishop A R 2010 Stable structures with high topological charge in nonlinear photonic quasicrystals *Phys. Rev. A* **82** 035802
[47] Ablowitz M J, Antar N, Bakírtaş İ and Ilan B 2012 Vortex and dipole solitons in complex two-dimensional nonlinear lattices *Phys. Rev. A* **86** 033804
[48] Antar N 2014 Pseudospectral renormalization method for solitons in quasicrystal lattice with the cubic-quintic nonlinearity *J. Appl. Math.* **2014** 848153
[49] Sbroscia M, Viebahn K, Carter E, Yu J C, Gaunt A and Schneider U 2020 Observing localization in a 2D quasicrystalline optical lattice *Phys. Rev. Lett.* **125** 200604
[50] Harris W F 1977 Disclinations *Sci. Am.* **237** 130–45
[51] Bohsung J and Trebin H R 1987 Disclinations in quasicrystals *Phys. Rev. Lett.* **58** 2277–80
[52] Kleman M and Friedel J 2008 Disclinations, dislocations and continuous defects: a reappraisal *Rev. Mod. Phys.* **80** 61–115
[53] Lin Z K, Wang Q, Liu Y, Xue H, Zhang B, Chong Y and Jiang J H 2023 Topological phenomena at defects in acoustic, photonic and solid-state lattices *Nat. Rev. Phys.* **5** 483–95
[54] Peterson C W, Li T, Jiang W, Hughes T L and Bahl G 2021 Trapped fractional charges at bulk defects in topological insulators *Nature* **589** 376–80
[55] Liu Y, Leung S, Li F F, Lin Z K, Tao X, Poo Y and Jiang J H 2021 Bulk-disclination correspondence in topological crystalline insulators *Nature* **589** 381–5
[56] Ren B, Wang H, Kartashov Y V, Li Y and Zhang Y 2023 Nonlinear photonic disclination states *APL Photon.* **8** 016101
[57] Xavier J, Boguslawski M, Rose P, Joseph J and Denz C 2010 Reconfigurable optically induced quasicrystallographic three-dimensional complex nonlinear photonic lattice structures *Adv. Mater.* **22** 356–60
[58] Boguslawski M, Rose P and Denz C 2011 Increasing the structural variety of discrete nondiffracting wave fields *Phys. Rev. A* **84** 013832
[59] Li C, Qin X, Liu K, Zhang H, Zhou Y, Tai Y and Li X 2025 Optical vortex in a quasicrystal structure *Opt. Lett.* **50** 3373–6
[60] Szameit A and Nolte S 2010 Discrete optics in femtosecond-laser-written photonic structures *J. Phys. B: At. Mol. Opt. Phys.* **43** 163001
[61] Mahmood R, Ramirez A V and Hillier A C 2021 Creating two-dimensional quasicrystal, supercell and moiré lattices with laser interference lithography: implications for photonic bandgap materials *ACS Appl. Nano Mater.* **4** 8851–62
[62] Kirsch M S, Zhang Y, Kremer M, Maczewsky L J, Ivanov S K, Kartashov Y V, Torner L, Bauer D, Szameit A and Heinrich M 2021 Nonlinear second-order photonic topological insulators *Nat. Phys.* **17** 995–1000
[63] Arkhipova A A *et al* 2023 Observation of π solitons in oscillating waveguide arrays *Sci. Bull.* **68** 2017–24
[64] Ren B *et al* 2023 Observation of nonlinear disclination states *Light Sci. Appl.* **12** 194
[65] Zhong H *et al* 2024 Observation of nonlinear fractal higher order topological insulator *Light Sci. Appl.* **13** 264
[66] Kompanets V O *et al* 2025 Observation of nonlinear topological corner states originating from different spectral charges *Adv. Mater.* **37** 2500556
[67] Skryabin N, Zhuravitskii S, Dyakonov I, Straupe S, Kalinkin A and Kulik S 2024 Femtosecond-laser-written low-loss multiscan waveguides in fused silica *Phys. Rev. Appl.* **22** 064079
[68] Zhang B, Yan W and Chen F 2025 Recent advances in femtosecond laser direct writing of three-dimensional periodic photonic structures in transparent materials *Adv. Photon.* **7** 034002
[69] Fleischer J W, Segev M, Efremidis N K and Christodoulides D N 2003 Observation of two-dimensional discrete solitons in optically induced nonlinear photonic lattices *Nature* **422** 147–50
[70] Schwartz T, Bartal G, Fishman S and Segev M 2007 Transport and Anderson localization in disordered two-dimensional photonic lattices *Nature* **446** 52–55
[71] Chen Z, Segev M and Christodoulides D N 2012 Optical spatial solitons: historical overview and recent advances *Rep. Prog. Phys.* **75** 086401
[72] Zhong H, Xia S, Zhang Y, Li Y, Song D, Liu C and Chen Z 2021 Nonlinear topological valley Hall edge states arising from type-II Dirac cones *Adv. Photon.* **3** 056001

[73] Zhang Z Y et al 2020 Observation of edge solitons in photonic graphene Nat. Commun. 11 1902
[74] Zhang Z, Liang S, Septembre I, Yu J, Huang Y, Liu M, Zhang Y, Xiao M, Malpuech G and Solnyshkov D 2024 Non-Hermitian delocalization in a two-dimensional photonic quasicrystal Phys. Rev. Lett. 132 263801
[75] Maciá E 2012 Exploiting aperiodic designs in nanophotonic devices Rep. Prog. Phys. 75 036502
[76] Hwang M S, Kim H R, Kim J, Yang B J, Kivshar Y and Park H G 2024 Vortex nanolaser based on a photonic disclination cavity Nat. Photon. 18 286–93